PLANT SCIENCE

Plant PIEZO homologs modulate vacuole morphology during tip growth

Ivan Radin[1], Ryan A. Richardson[1], Joshua H. Coomey[1], Ethan R. Weiner[1]†, Carlisle S. Bascom[2]‡, Ting Li[3], Magdalena Bezanilla[2], Elizabeth S. Haswell[1]*

In animals, PIEZOs are plasma membrane–localized cation channels involved in diverse mechanosensory processes. We investigated PIEZO function in tip-growing cells in the moss *Physcomitrium patens* and the flowering plant *Arabidopsis thaliana*. *Pp*PIEZO1 and *Pp*PIEZO2 redundantly contribute to the normal growth, size, and cytoplasmic calcium oscillations of caulonemal cells. Both *Pp*PIEZO1 and *Pp*PIEZO2 localized to vacuolar membranes. Loss-of-function, gain-of-function, and overexpression mutants revealed that moss PIEZO homologs promote increased complexity of vacuolar membranes through tubulation, internalization, and/or fission. *Arabidopsis* PIEZO1 also localized to the tonoplast and is required for vacuole tubulation in the tips of pollen tubes. We propose that in plant cells the tonoplast has more freedom of movement than the plasma membrane, making it a more effective location for mechanosensory proteins.

The ability to sense and respond to mechanical forces such as gravity, touch, or cell swelling is an ancient property essential for normal cellular function (*1*). Externally or internally derived forces can lead to increased lateral membrane tension, activating mechanosensitive channels and leading to the flow of ions down their electrochemical gradients (*2*–*4*). In animal cells, members of the PIEZO family of mechanosensitive ion channels form trimeric complexes that conduct calcium and are embedded in the plasma membrane (*5*–*7*). PIEZO channels are required for perception of light touch, shear stress, compressive force, proprioception, brain development, and nociception in animals (*6*, *7*).

PIEZO channel homologs are found throughout eukaryotic genomes (*5*, *8*, *9*). *At*PIEZO1, from the model flowering plant *Arabidopsis thaliana,* is required to control the systemic spread of viruses (*9*) and is implicated in root cap mechanotransduction (*10*, *11*). How PIEZO channels might function in plants presents a puzzle given the biomechanics of the plant cell. Plant cells are surrounded by a sturdy yet flexible cell wall and have an osmotic pressure up to 1000 times that of animal cells. We investigated PIEZO homologs in the moss *Physcomitrium* (formerly *Physcomitrella*) *patens* and the flowering dicot *A. thaliana*.

Our phylogenetic analyses indicate that PIEZO homologs likely descended from a single ancestor and underwent multiple independent duplications and losses throughout *Eukaryota* (Fig. 1A, figs. S1 and S2, and table S1). The two moss homologs *Pp*PIEZO1 (Pp3c9_13300V3.1) and *Pp*PIEZO2 (Pp3c3_17170V3.1) are the products of an independent duplication of ancestral PIEZO (one of four within the green lineage) (Fig. 1A and fig. S1). With CRISPR-Cas9 gene editing, we generated both single (Δ*PP1-I*, Δ*PP1-II*, Δ*PP2-I*, and Δ*PP2-II*, for *Physcomitrium* PIEZO) and double (Δ*PP1/2-I* and Δ*PP1/2-II*) mutants (fig. S3A). All plant lines and mutant alleles are described in table S2. When cultured on standard media with cellophane, Δ*PP1* and Δ*PP2* single-mutant plants were similar in size to the wild type (WT), but double Δ*PP1/2* mutants were significantly smaller (Fig. 1B and fig. S3B). In Δ*PP1/2* mutants, the filaments that spread away from the edge of the main plant

[1]Department of Biology and NSF Center for Engineering Mechanobiology, Washington University in St. Louis, St. Louis, MO, USA. [2]Department of Biological Sciences, Dartmouth College, NH, USA. [3]Division of Biology and Biological Engineering, California Institute of Technology, Pasadena, CA, USA.
*Corresponding author. Email: ehaswell@wustl.edu
†Present address: Department of Botany, University of Wisconsin–Madison, WI, USA. ‡Present address: Division of Biological Sciences, University of California, San Diego, CA, USA.

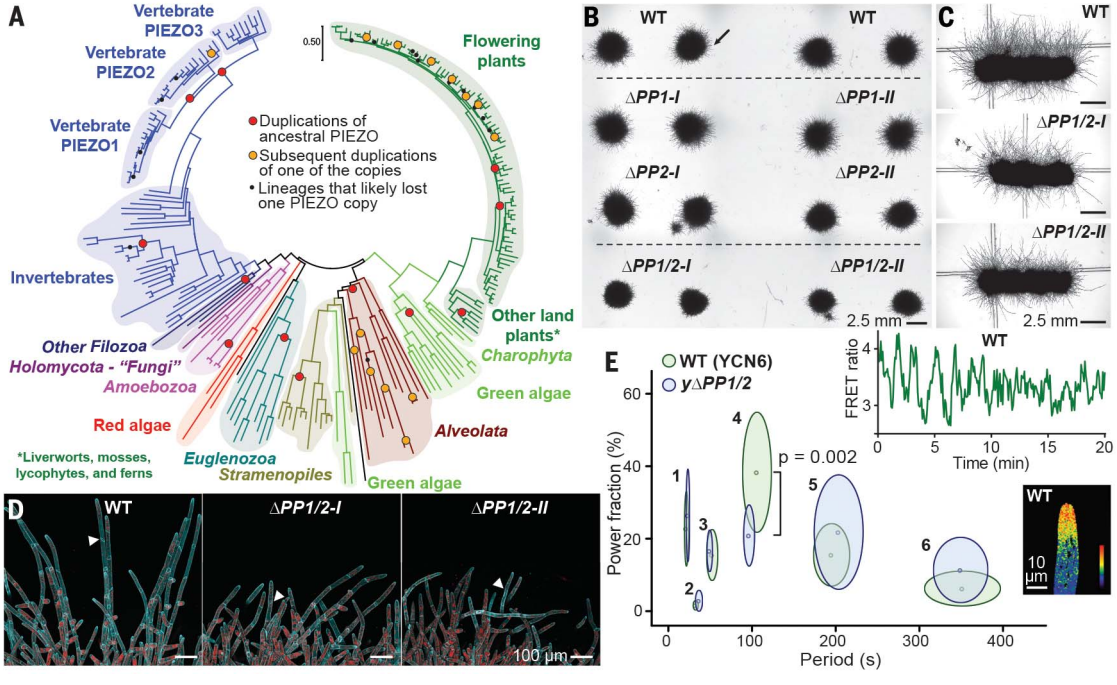

Fig. 1. Moss PIEZO homologs are required for normal cell growth and cytosolic calcium oscillations. (**A**) Maximum likelihood phylogenetic tree of the PIEZO family on the basis of protein sequences of conserved PIEZO domains from 235 homologs. (**B**) Moss from fragmented protonema after 7 days of growth on cellophaned media. (**C**) Plants grown in the dark for 10 days. (**D**) Deconvolved Z-maximum intensity projections of cells from the plant edge [black arrow in (B)]. Cell wall dye calcofluor white, cyan; chlorophyll autofluorescence, red. Arrowheads point out oblique cross walls, the identifying characteristic of caulonemal cells. (**E**) Period–power fraction plot of intrinsic mode functions identified in complex Ca^{2+} oscillation signals from WT (n = 12) and *yΔPP1/2* (n = 14) caulonemal cells. Circles, mean values; ovals, standard error. (Inset) WT Ca^{2+} signal and recorded tip oscillations. FRET, fluorescence resonance energy transfer. In the color bar of cytosolic Ca^{2+} levels: red, high; blue, low. Statistics, Mann-Whitney test ($P < 0.05$).

were shorter and less abundant under both light and dark growth conditions (Fig. 1, B to D, and fig. S3C). Light-grown Δ*PP1/2* caulonemal cells grew more slowly, and Δ*PP1/2* subapical caulonemal cells were shorter and curvier than the WT (Fig. 1D and fig. S3, D and E). A third independently generated Δ*PP1/2* mutant line showed similar growth defects (fig. S3F). Descriptive statistics for all graphs are given in table S3.

We next evaluated the contribution of *Pp*PIEZOs to cytoplasmic Ca^{2+} fluctuations in the tips of growing caulonemal cells. When moss is grown in microfluidic chambers, the complex tipward Ca^{2+} oscillations of apical caulonemal cells can be imaged and decomposed into six frequencies referred to as intrinsic mode functions (IMFs) (*12*). We found that IMF4 was significantly reduced in Δ*PP1/2* mutants compared with the WT (Fig. 1E and fig. S4, A to C). Thus, PIEZOs contribute to the cytoplasmic Ca^{2+} signature in moss. The Ca^{2+} oscillation defect in Δ*PP1/2* mutants could be a secondary effect of their altered growth. However, the growth rate of *y*Δ*PP1/2* cells in microfluidic chambers did not correlate with the changes in Ca^{2+} oscillations (fig. S4, D and E).

Although animal PIEZOs localized to the plasma membrane (*7, 13*), we found that *Pp*PIEZOs did not. Codon-optimized o*Pp*PIEZO1 and o*Pp*PIEZO2 tagged with monomeric enhanced GFP (mGFP) localized to the vacuolar membrane (tonoplast) when transiently overexpressed in protoplasts (Fig. 2A). Genomic integration of the same overexpression constructs produced full-length fusion proteins (fig. S5A), with a localization pattern consistent with vacuolar targeting (Fig. 2B). To confirm vacuolar localization under native expression levels, *mGFP* was integrated into the *PpPIEZO1/2* native loci to make *gPpPIEZO1-mGFP* and *gPpPIEZO2-mGFP* lines (fig. S3A). Full length fusion proteins were detected by immunoblotting (Fig. 2C), and no phenotypic differences from the WT were observed in these lines (fig. S5B). g*Pp*PIEZO1/2-mGFP localized to the tonoplast in subapical and apical caulonemal cells, as well as chloronemal cells (Fig. 2D and fig. S5, C and D). To establish the orientation of *Pp*PIEZOs within the tonoplast, we employed a bimolecular fluorescence complementation assay. The results indicated that the C termini of both *Pp*PIEZOs face the cytosol (Fig. 2, E and F, and fig. S6), which is analogous to animal PIEZOs (*7*) and supports a model in which *Pp*PIEZOs release Ca^{2+} into the cytoplasm from the vacuolar stores (*14*).

Vacuoles perform many essential functions in plant cells (*13*), and their morphology changes dynamically in response to internal and external cues (*15*). Given the localization of *Pp*PIEZOs to the vacuole, we investigated vacuolar morphology in caulonemal cells in the WT and mutant lines. We combined brightfield imaging and staining with either 5(6)carboxy2′,7′-dichlorofluorescein diacetate (carboxy-DCFDA), which stains the vacuolar lumen, or MDY-64, which stains the tonoplast, among other compartments (Fig. 3A and fig. S7A). In WT caulonemal cells, the apical region between the nucleus and tip is characterized by highly tubulated and fragmented vacuoles; by contrast, the vacuoles in the basal region are tubule-like in younger cells (fig. S7B) but are fused and expanded in

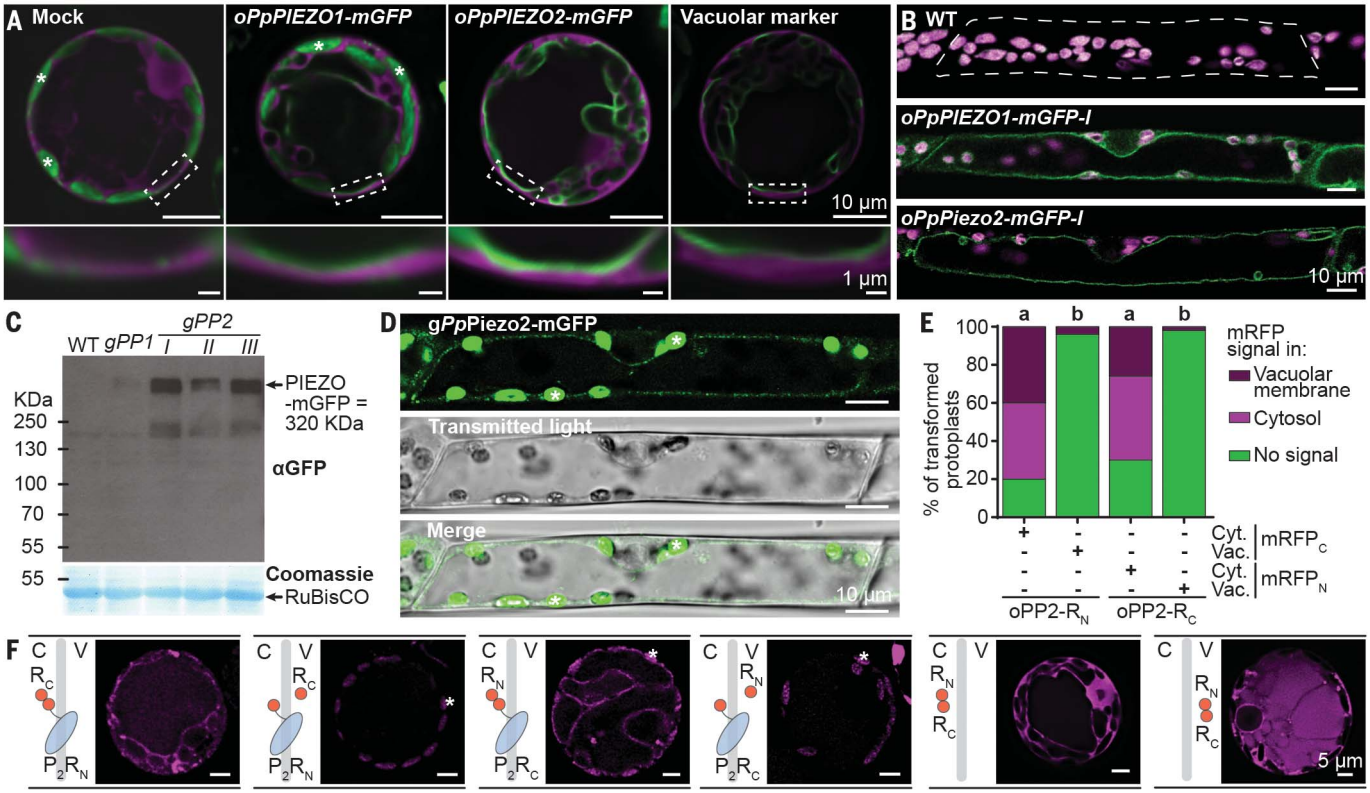

Fig. 2. *Pp*PIEZO proteins localize to the vacuolar membrane with cytosolic C termini. (**A**) WT protoplasts transiently expressing cytosolic *mCherry* (magenta) and *UBQ::oPpPIEZO1-mGFP*, *UBQ::oPpPIEZO2-mGFP*, or vacuolar marker *Vam3-mGFP* (green). Dashed boxes in (A) are magnified in the bottom panels. (**B**) Subapical caulonemal cells stably expressing the same constructs as in (A) (green, mGFP; magenta, chlorophyll autofluorescence). (**C**) Immunoblot of total protein extracts showing the presence of full-length fusion proteins. (**D**) Subapical caulonemal cell from mGFP knock-in lines. (**E** and **F**) WT protoplasts expressing o*Pp*PIEZO2 (P_2) C-terminally tagged with either the N- or C-terminal half of mRFP (indicated by R_N or R_C); the other half of mRFP is targeted to the cytosol (indicated by C) or vacuolar lumen (indicated by V). mRFP fluorescence, magenta. $n = 50$. Statistics, Fisher's exact test ($P < 0.05$). Asterisks, chlorophyll autofluorescence. All images are from a single deconvolved focal plane.

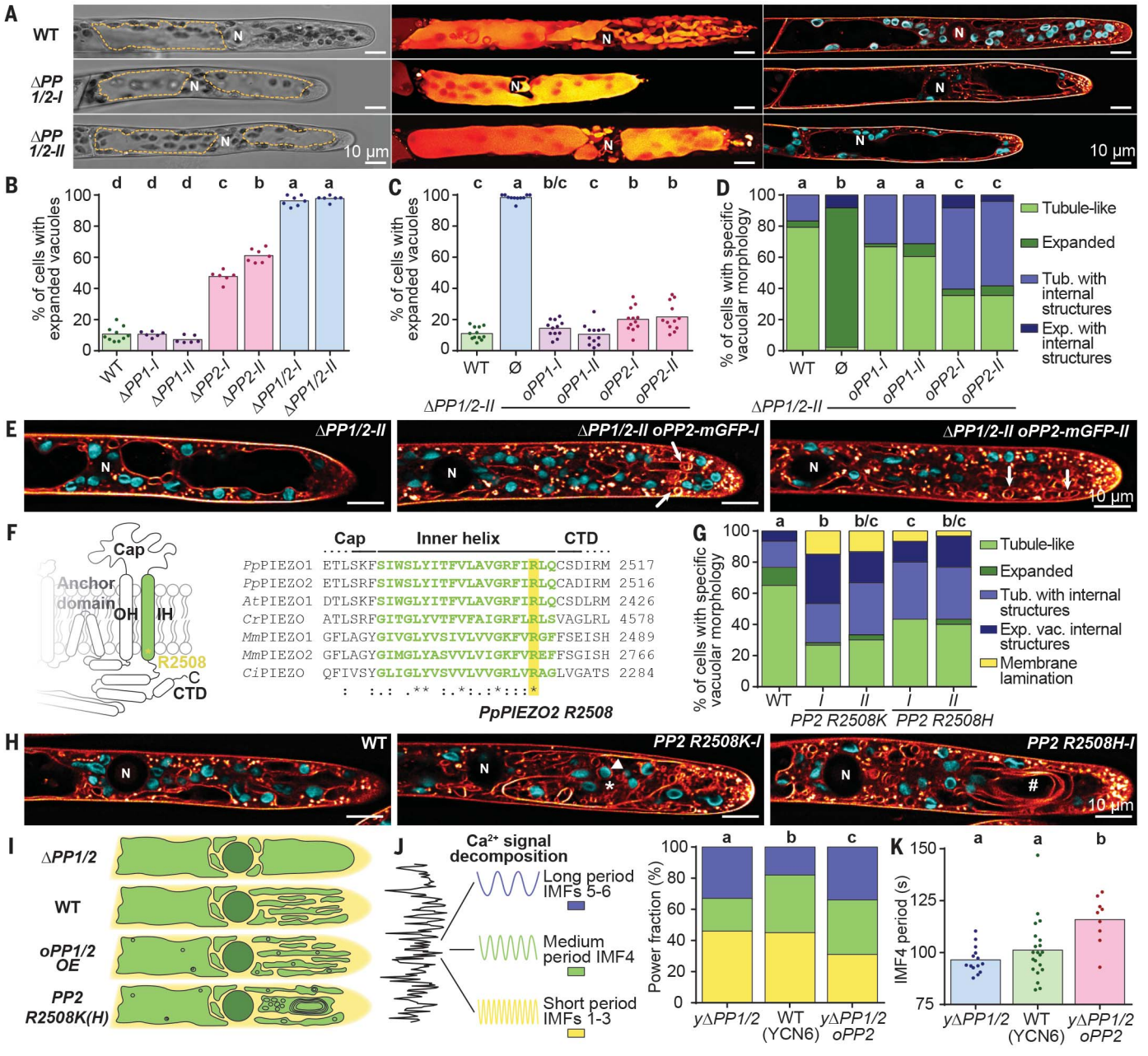

Fig. 3. *Pp*PIEZO1 and *Pp*PIEZO2 modulate vacuolar morphology. (**A**) Apical caulonemal cells: (left) brightfield images (yellow lines indicate expanded vacuoles); (middle) stained with carboxy-DCFDA (Z-maximum intensity projections); (right) stained with MDY64 (orange; chlorophyll autofluorescence, cyan). (**B**) Percentage of cells with expanded vacuoles in the apical region. Statistics, one-way ANOVA with post-hoc Tukey test ($P < 0.05$). (**C**) The vacuolar phenotype of cells overexpressing *oPP1/oPP2-mGFP*. Statistics same as in (B). (**D** and **E**) Vacuolar phenotypes of *oPP1/oPP2* overexpression cells ($n = 48$). Statistics, Fisher's exact test ($P < 0.05$). (**F**) PIEZO pore module and alignment of inner helix protein sequences (*At*, *Arabidopsis*; *Pp*, moss; *Mm*, mouse, *Cr*, *Chlamydomonas reinhardtii*; *Ci*, *Ciona intestinalis*). Single-letter abbreviations for the amino acid residues are as follows: A, Ala; C, Cys; D, Asp; E, Glu; F, Phe; G, Gly; H, His; I, Ile; K, Lys; L, Leu; M, Met; N, Asn; P, Pro; Q, Gln; R, Arg; S, Ser; T, Thr; V, Val; W, Trp; and Y, Tyr. (**G** and **H**) Vacuolar phenotypes of *PpPIEZO2* point mutants ($n = 60$). Statistics same as in (D). (**I**) Graphic summary of vacuolar morphologies observed in different moss lines. OE, overexpression. (**J**) Ratio of intrinsic mode functions (IMFs) identified in Ca^{2+} oscillatory profiles. Statistics, chi-square test ($P < 0.05$). (**K**) Periods associated with IMF4. Statistics, Kruskal-Wallis test with Dunn's multiple comparisons test ($P < 0.05$). (J, K) Graphs contain combined data from figs. S4, B and C, and S10, D and E. All images are from a single deconvolved focal plane, except the middle images in (A). Arrows, tubule-like vacuoles with internal structures; asterisks, expanded vacuoles with internal structures; number signs, expanded vacuoles with membrane lamination; arrowheads, internalized chloroplasts. N, nucleus.

mature cells (Fig. 3A and fig. S7C). We found that *ΔPP1/2* mutants had large, expanded vacuoles in both apical and basal regions in >95% of caulonemal tip cells (Fig. 3, A and B, and fig. S7, A to D). This vacuolar phenotype was independent of growth rate (fig. S7E) and could be rescued by overexpression of *oPpPIEZO1/2-mGFP* (Fig. 3C and fig. S8). The vacuolar morphology of apical caulonemal cells from *gPpPIEZO1-mGFP* and *gPpPIEZO2-mGFP* lines was normal (fig. S9), confirming that GFP tagging did not alter protein function. Thus,

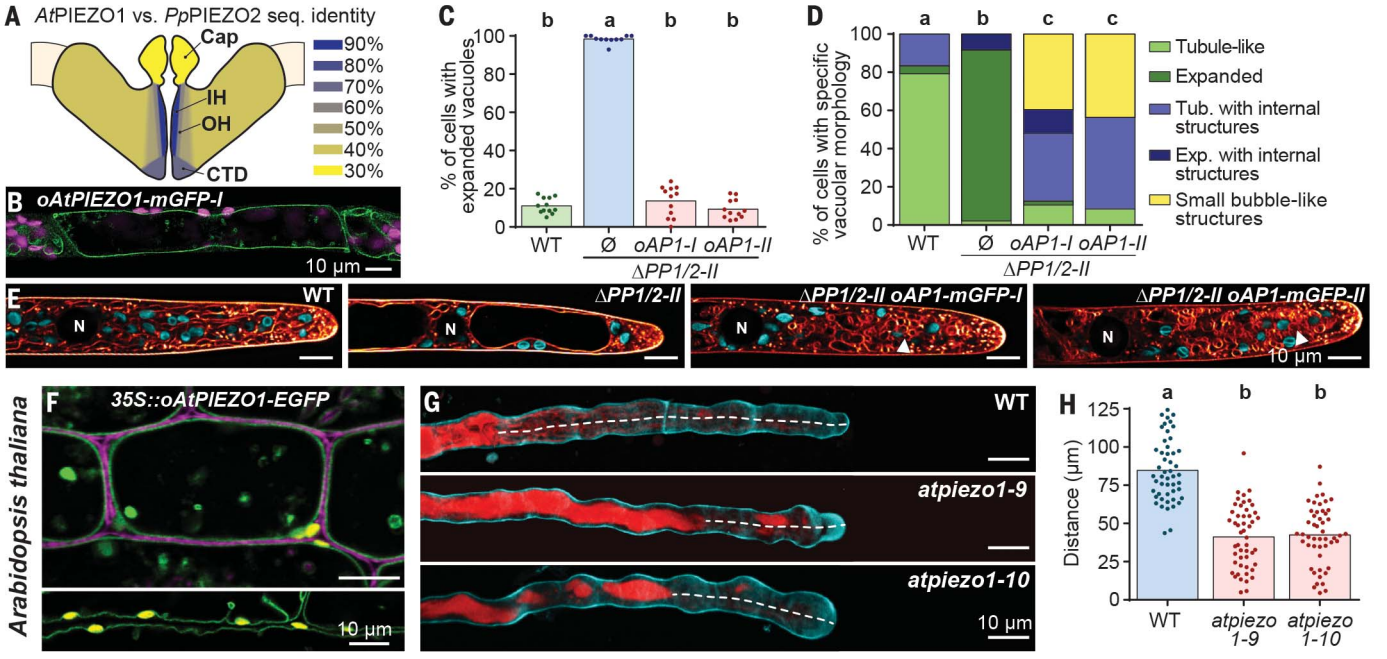

Fig. 4. *Arabidopsis* PIEZO1 localizes to the vacuole and modulates the vacuolar morphology. (**A**) Protein sequence identity between *At*PIEZO1 and *Pp*PIEZO2 (not to scale). (**B**) Subapical Δ*PP1/2-II* caulonemal cells stably expressing *UBQ::oAtPIEZO1-mGFP* (*oAT1*). Green, mGFP; magenta, chlorophyll autofluorescence. (**C**) Suppression of Δ*PP1/2-II* expanded vacuole phenotype by *At*PIEZO1. Statistics, one-way ANOVA with post-hoc Tukey test ($P < 0.05$). (**D** and **E**) Vacuolar phenotypes of apical caulonemal cells stained with MDY64 ($n = 48$). Statistics, Fisher's exact test ($P < 0.05$). Data for WT and Δ*PP1/2-II* in (C) and (D) are repeated from Fig. 3, C and D, respectively. (**F**) *Arabidopsis* hypocotyl cells (top) and intersection of three petiole cells (bottom) stably expressing *35S::oAtPIEZO1-EGFP*. Green, EGFP; yellow, chlorophyll autofluorescence; magenta, plasma membrane marker pm-RK. (**G**) Z maximum projection images of pollen tubes stained with calcofluor white (cyan) and BCECF (red). White lines indicate the distance between tube tip and expanded vacuoles, which is quantified in (H). Statistics same as (C). All images are from a single deconvolved focal plane, except in (G). N, nucleus.

*Pp*PIEZOs are required for tubulated vacuoles in the apical region of caulonemal cells.

In some cases, *oPpPIEZO1/2-mGFP* lines exhibited an increased number of intravacuolar structures throughout the apical caulonemal cells [Fig. 3, D and E (arrows) and fig. S10]. To further investigate the effect of increased *Pp*PIEZO function, we were inspired by two gain-of-function mutations in animal PIEZOs associated with disease and altered channel function (*7*). As the affected residues are conserved in plant PIEZOs (Fig. 3F), we introduced three analogous changes (R2508K, R2508H, and E2548del) into the *PpPIEZO2* native loci (fig. S3A). Although *PP2 R2508K* and *PP2 R2508H* plants did not have obvious growth defects (fig. S11A), 60 to 70% of their apical caulonemal cells contained intravacuolar structures seldom seen in WT cells, as well as a membrane lamination phenotype not seen in WT cells (Fig. 3, G and H, and fig. S11B). In some cases, chloroplasts and cytoplasm were internalized within vacuoles (Fig. 3H, arrowhead). Large vacuoles in the basal region of the apical caulonemal cells also had intravacuolar membrane structures (fig. S11C). The *PP2 E2549del* lines produced a loss-of-function phenotype similar to that of Δ*PP2* mutants (fig. S12). Thus, both loss- and gain-of-function alleles indicate that *Pp*PIEZOs influence vacuolar fission and/or tonoplast invagination (Fig. 3I).

When grown on solid media, most cells of the *yΔPP1/2* mutant line used for Ca^{2+} imaging had expanded vacuoles (fig. S13A). However, under microfluidic growth conditions, about half had vacuoles similar to those in the WT, providing an opportunity to explore the relationship between vacuole morphology and Ca^{2+} oscillations. When we compared Ca^{2+} oscillations in WT and *yΔPP1/2* cells with similar vacuolar morphology, we found a statistically significant difference in IMF4 (fig. S13B), indicating that the effect of *Pp*PIEZOs on IMF4 is independent of vacuolar morphology. Overexpression of o*Pp*PIEZO2-mGFP in a *yΔPP1/2* background restored the power fraction of IMF4 to WT levels but reduced the power fraction of short period IMFs and increased IMF4's average period (Fig. 3, J and K, and fig. S13, C to E). Altogether, our data show that *Pp*PIEZOs affect cytosolic Ca^{2+} oscillatory profiles.

To determine whether these characteristics are exclusive to moss PIEZOs, we investigated the localization and function of *At*PIEZO1 (At2g48060) (Fig. 4A). When full-length oAtPIEZO1-mGFP was overexpressed (using the maize UBIQUITIN promoter) in moss cells, it localized to the tonoplast and suppressed the expanded vacuole phenotype. It also suppressed some of the growth defects of the Δ*PP1/2* mutants (Fig. 4, B and C, and fig. S14, A and B). We observed intravacuolar membrane structures throughout apical caulonemal cells in these lines three to four times more often than in the WT (Fig. 4, D and E, and fig. S14, C and D). In ~40% of these cells, we also observed a new phenotype in which vacuoles appeared as small, bubble-like structures that filled the cytoplasm (Fig. 4E and fig. S14C, arrowheads). Full-length o*At*PIEZO1-EGFP expressed in *Arabidopsis* localized to the vacuole in hypocotyl and petiole cells (Fig. 4F and fig. S15, A and B).

*At*PIEZO1 is expressed in most plant tissues, including pollen grains and tubes (*16*). Pollen tubes are a well-studied model system for tip growth in flowering plants (*17*) and are characterized by tubule-like vacuoles in the tip region (*18*). We compared the vacuolar morphology of in vitro germinated pollen tubes from the WT and two *AtPIEZO1* CRISPR-Cas9 mutant lines (*atpiezo1-9* and *atpiezo1-10*; tables S2 and S4 and fig. S15C). We observed expanded vacuoles in both mutants (Fig. 4G and fig. S15D). The first expanded vacuole in a WT pollen tube was located 80 micrometers

(on average) from the tube tip, but the expanded vacuoles in the *atpiezo1* mutant pollen tubes were only 40 micrometers (on average) from the tip (Fig. 4, G and H). Pollen grains and tubes from the *atpiezo1* plants did not have any discernible defects (fig. S15, E to I), perhaps as a result of redundancy with TPK1, another tonoplast MS ion channel (*19*). Thus, so far as moss and *Arabidopsis* can be used as proxies for their lineages, PIEZO localization to the vacuole membrane and the role of PIEZOs in promoting vacuolar fission and/or invagination in tip-growing cells are conserved among land plants.

Vacuole remodeling has been linked to mechanosensing in plant cells (*20*) and occurs in response to high $[Ca^{2+}]_{cyt}$ in yeast (*21*). We speculate that *Pp*PIEZOs release Ca^{2+} into the cytoplasm from vacuolar stores in response to the physical state of the tonoplast, which in turn leads to increased vacuolar fission and/or internalization (fig. S16). During WT tip growth, an increase in vacuole surface volume in apical cells may allow these exploratory cells to grow more efficiently or better adapt to local changes in their environment. In the plant lineage, PIEZO homologs may have been coopted to sense the mechanical status of plant tonoplasts, including turgor. This relocation to the vacuole may reflect a higher freedom of movement of vacuolar membranes compared with the plasma membrane, making the tonoplast a preferred location for sensing and responding to changes in plant cell mechanics.

REFERENCES AND NOTES

1. A. Anishkin, S. H. Loukin, J. Teng, C. Kung, *Proc. Natl. Acad. Sci. U.S.A.* **111**, 7898–7905 (2014).
2. S. S. Ranade, R. Syeda, A. Patapoutian, *Neuron* **87**, 1162–1179 (2015).
3. D. Basu, E. S. Haswell, *Curr. Opin. Plant Biol.* **40**, 43–48 (2017).
4. C. D. Cox, N. Bavi, B. Martinac, *Annu. Rev. Physiol.* **80**, 71–93 (2018).
5. B. Coste *et al.*, *Science* **330**, 55–60 (2010).
6. S. N. Bagriantsev, E. O. Gracheva, P. G. Gallagher, *J. Biol. Chem.* **289**, 31673–31681 (2014).
7. J. Wu, A. H. Lewis, J. Grandl, *Trends Biochem. Sci.* **42**, 57–71 (2017).
8. D. L. Prole, C. W. Taylor, *PLOS ONE* **8**, e66068 (2013).
9. Z. Zhang *et al.*, *Sci. Rep.* **9**, 3187 (2019).
10. X. Fang *et al.*, *Int. J. Mol. Sci.* **22**, 467 (2021).
11. S. A. R. Mousavi *et al.*, *Proc. Natl. Acad. Sci. U.S.A.* **118**, e2102188118 (2021).
12. C. S. Bascom Jr., L. J. Winship, M. Bezanilla, *Proc. Natl. Acad. Sci. U.S.A.* **115**, E2869–E2878 (2018).
13. X. Tan *et al.*, *Plants* **8**, 327 (2019).
14. G. Schönknecht, *Plants* **2**, 589–614 (2013).
15. Y. Cui, Q. Zhao, S. Hu, L. Jiang, *Trends Plant Sci.* **25**, 538–548 (2020).
16. J. Waese, N. J. Provart, in *Plant Genomics Databases: Methods and Protocols*, A. D. J. van Dijk, Ed. (Springer, 2017), pp. 119–148.
17. N. Scheible, A. McCubbin, *Plants* **8**, 156 (2019).
18. G. R. Hicks, E. Rojo, S. Hong, D. G. Carter, N. V. Raikhel, *Plant Physiol.* **134**, 1227–1239 (2004).
19. F. J. M. Maathuis, *New Phytol.* **191**, 84–91 (2011).
20. K. Dünser *et al.*, *EMBO J.* **38**, e100353 (2019).
21. R. Kellermayer, D. P. Aiello, A. Miseta, D. M. Bedwell, *J. Cell Sci.* **116**, 1637–1646 (2003).

ACKNOWLEDGMENTS

We thank S.-Z. Wu for generating the Vam3-GFP vacuolar marker, S. Ryken for help with calcium imaging, S.A.R. Mousavi and A. Patapoutian for codon-optimized *AtPIEZO1* and helpful discussions, and E. Meyerowitz for the *Arabidopsis thaliana* CRISPR lines. **Funding:** E.S.H. received HHMI-Simons Faculty Scholar Grant 55108530, NSF MCB-1929355, and funding from the NSF Center for Engineering Mechanobiology. M.B. received NSF MCB-1330171. **Author contributions:** I.R., R.A.R., J.H.C., E.R.W., M.B., and E.S.H. designed and performed the experiments and analyzed the data. I.R., M.B., and E.S.H. wrote the paper. T.L. and C.S.B. created some of the reagents. **Competing interests:** The authors declare no competing interests. **Data and materials availability:** All data are available in the manuscript and supplementary materials.

SUPPLEMENTARY MATERIALS

science.sciencemag.org/content/373/6554//586/suppl/DC1
Materials and Methods
Figs. S1 to S16
Tables S1 to S4
References (*22*–*54*)
MDAR Reproducibility Checklist

View/request a protocol for this paper from *Bio-protocol*.

3 September 2020; resubmitted 24 February 2021
Accepted 16 June 2021
10.1126/science.abe6310

Science

Plant PIEZO homologs modulate vacuole morphology during tip growth

Ivan RadinRyan A. RichardsonJoshua H. CoomeyEthan R. WeinerCarlisle S. BascomTing LiMagdalena BezanillaElizabeth S. Haswell

Science, 373 (6554), • DOI: 10.1126/science.abe6310

Plant cell growth regulation

Piezo sensors in animal cells are localized in the cell membrane and transduce mechanical signals. The cell membrane of plant cells, unlike that of animal cells, is usually plastered up against a stiff cell wall and does not have much mobility. Much of the cell's volume is accounted for by a large central vacuole, the membrane of which, the tonoplast, is not so mechanically constrained. Radin *et al*. studied how and where plant cells use Piezo sensors. Plant homologs of the animal mechanosensitive channels are found not in the plasma membrane but rather in the tonoplast. In both moss and the small flowering plant *Arabidopsis*, mutations in plant Piezo sensors altered vacuolar morphology and growth patterns in tip-growing cells. —PJH